ResearchGate

See discussions, stats, and author profiles for this publication at: https://www.researchgate.net/publication/49804684

Hydrophobic, Aromatic, and Electrostatic Interactions Play a Central Role in Amyloid Fibril Formation and Stability

ARTICLE *in* BIOCHEMISTRY · FEBRUARY 2011

Impact Factor: 3.02 · DOI: 10.1021/bi101936c · Source: PubMed

CITATIONS
62

READS
59

7 AUTHORS, INCLUDING:

Karen E Marshall
University of Sussex
11 PUBLICATIONS **385** CITATIONS
SEE PROFILE

Kyle L Morris
The University of Warwick
25 PUBLICATIONS **1,059** CITATIONS
SEE PROFILE

Laurence Lewis
Max Planck Institute of Neurobiology
4 PUBLICATIONS **119** CITATIONS
SEE PROFILE

Helen Walden
University of Dundee
28 PUBLICATIONS **1,434** CITATIONS
SEE PROFILE

Available from: Laurence Lewis
Retrieved on: 24 January 2016

BIOCHEMISTRY
including biophysical chemistry & molecular biology

ARTICLE

pubs.acs.org/biochemistry

Hydrophobic, Aromatic, and Electrostatic Interactions Play a Central Role in Amyloid Fibril Formation and Stability

Karen E. Marshall,[†,§] Kyle L. Morris,[†] Deborah Charlton,[†] Nicola O'Reilly,[‡] Laurence Lewis,[‡] Helen Walden,[‡] and Louise C. Serpell*[,†]

[†]School of Life Sciences, University of Sussex, Falmer, East Sussex BN1 9QG, U.K.

[‡]Protein Structure and Function Laboratory, Lincoln's Inn Fields Laboratories, London Research Institute of Cancer Research UK, 44 Lincoln's Inn Fields, London WC2A 3LY, U.K.

Supporting Information

ABSTRACT: Amyloid-like fibrous crystals formed by the peptide KFFEAAAKKFFE have been previously characterized and provide an ideal model system to examine the importance of specific interactions by introducing specific substitutions. We find that the removal of any phenylalanine residue completely abrogates assembly ability, while charged residues modulate interactions within the structure resulting in alternative fibrillar morphologies. X-ray fiber diffraction analysis reveals that the essential backbone packing of the peptide molecules is maintained, while small changes accommodate differences in side chain size in the variants. We conclude that even very short peptides are adaptable and add to the growing knowledge regarding amyloid polymorphisms. Additionally, this work impacts on our understanding of the importance of residue composition for amyloidogenic peptides, in particular the roles of electrostatic, aromatic, and hydrophobic interactions in amyloid assembly.

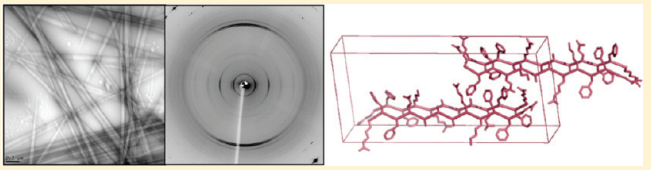

Amyloid fibers are highly ordered, stable protein aggregates that share common structural and staining characteristics, despite being composed of proteins or peptides with little or no obvious sequence homology. *In Vivo*, amyloid often presents as a pathological hallmark of certain diseases such as Alzheimer's disease, in which the self-assembly of the natively unfolded 40 or 42 residue peptide Aβ into amyloid is associated with disease progression.[1] More recently, examples have emerged that suggest a nonpathogenic role for amyloid. These include curli fibers produced by *Escherichia coli* that aid in adhesion of the bacterium to surfaces and stain with the amyloid specific Congo Red dye and yeast and fungal prions (e.g., Sup35 and HET-s) that confer particular phenotypic traits to hosts.[2] Why some amyloid fibers are pathogenic and some are "useful" may be, at least in part, due to variations in structure.[3] Therefore, understanding particular sequence−structure−function relationships is likely to be essential in defining why certain amyloids exhibit characteristic activities.

Despite the lack of a clear sequence similarity between protein or peptide precursors, there is a generic conformation for amyloid known as cross-β, i.e., the perpendicular orientation of peptide strands respective to the fiber axis. It has been suggested that the ability to form amyloid is an inherent property of the polypeptide backbone and that any amino acid sequence would be able to form amyloid under particular conditions.[4] However, polymorphisms in amyloid indicate that while this proposition may be true, side chains do in fact play a fundamental role and may be responsible for the structural differences in fibers at an atomic level (side chain and peptide packing) or at a macromolecular level (protofilament packing). Therefore, sequence features may drive assembly into specific conformations while maintaining the overall cross-β arrangement.[5] Many disease-associated amyloid fibers are formed from large protein precursors that require a degree of unfolding before they can begin to self-assemble into amyloid.[6] Often these fibers contain a cross-β core composed of a limited number of residues that have been identified by hydrogen−deuterium exchange and limited proteolysis.[7−10] Isolated homologous peptide fragments are able to form amyloid fibers that show structural similarities to their parent proteins.[11] Fibers formed from these short peptides are often more amenable to biophysical analysis than those formed by larger precursors.[11−15] Furthermore, they can give more specific clues as to the roles of particular residues in assembly and structure. With this view in mind, we have used the well-characterized peptide KFFEAAAKKFFE[13] as a model system to investigate the influence of particular residues in structure and assembly using a combination of mutagenesis and analysis of the resulting structures using various biophysical methods.

KFFEAAAKKFFE is a designed peptide based on one of the shortest amyloid-forming peptides known, KFFE, linked by a flexible hydrophobic linker region.[16,17] The sequence contains features that are believed to increase the propensity to form amyloid and initiate aggregation, including FF pairs that feature in Aβ and serum amyloid A protein[13,18,19] and the motif AAXK, found in α-synuclein.[13] Previously, analysis of fibrous crystals

Received: December 4, 2010
Revised: January 31, 2011
Published: February 02, 2011

ACS Publications © 2011 American Chemical Society

formed by KFFEAAAKKFFE in phosphate-buffered saline (PBS) resulted in a high-resolution structural model.[13] The data were consistent with a model in which the extended β-strands run antiparallel to each other within a β-sheet, phenylalanine residues closely interlock in the sheet spacing direction and stack in the fiber axis direction, and electrostatic interactions are present between K1 and K9 on one peptide with E12 and E4, respectively, on the next β-strand down in the β-sheet. These electrostatic interactions are thought to stabilize the structure in the hydrogen-bonding or fiber axis direction and drive the antiparallel arrangement. The β-sheets associate laterally in the sheet-spacing direction and end to end, in the latter case possibly due to the positive and negative charges at the end of the peptides, forming a brick-like arrangement when viewed down the fiber axis (Supporting Information Figure S1).[13] Perpetuation of peptide association in each of these three dimensions is likely to be responsible for the crystalline nature of KFFEAAAKKFFE assemblies.

The high-resolution detail available for KFFEAAAKKFFE[13] (hereafter referred to as the WT sequence) makes it an ideal model system to assess the contribution from individual residues on assembly and structure. We initially investigated the influence from the phenylalanine residues and the previously proposed $\pi-\pi$ stacking by creating several variants in which either one or combinations of two phenylalanine residues were replaced with alanine. This replacement ensured that some hydrophobic character was maintained. Next, contributions to fibril formation from electrostatic interactions were investigated by constructing similar variants whereby lysine was replaced with alanine. The influence of smaller chemical changes on sequence was also investigated by creating a similar set of variants, except that lysine was replaced with arginine. Third, the role of charged ends in peptide association in the end-to-end lateral direction was explored using a peptide variant that had capped (uncharged) ends. The assembly and morphology of variants were monitored using electron microscopy. Intrinsic phenylalanine fluorescence from each of the variants was also examined to investigate aromatic stacking arrangements within the variants. Finally, X-ray fiber diffraction (FD) was carried out on fibrils formed by some of the variants to determine similarities and differences in the packing of the peptides within the structures formed compared to WT.

The results reveal important aspects regarding sequence determinants of amyloid assembly. In particular, they highlight a central role for the aromatic and hydrophobic phenylalanine residue in assembly propensity and the role of electrostatic interactions in mediating lateral association of protofilaments within the fibrils and fibrous crystals. These results demonstrate the dramatic effects amino acid sequence changes can have on amyloid forming propensity and resulting structure, particularly in relation to the contribution of phenylalanine in driving assembly and electrostatic and aromatic interactions in peptide packing.

EXPERIMENTAL PROCEDURES

Preparation of Peptides. Peptides used are shown in Table 1. NH_3^+-KFFEAAAKKFFE-COO^-, Ac-KFFEAAAKKFFE-NH_2, and F/A variants of KFFEAAAKKFFE were purchased as lyophilized powders from Bachem (St. Helens, U.K.) at >97% purity. K/A and K/R variants of KFFEAAAKKFFE were synthesized using 9-fluorenylmethyloxycarbonyl for temporary α-amino group protection and a low-loaded Wang resin preloaded with the C-terminal amino acid. Protecting groups used were Pbf (2,2,4,6,7-pentamethyldihydrobenzofuran-5-sulfonyl) for arginine, OtBu (−-butyl ester) for glutamic acid, and Boc (*tert*-butoxycarbonyl) for lysine. Each amino acid was coupled as a hydroxybenzotriazole active ester, automatically formed immediately prior to use. Automated synthesis took place on an Intavis Multipep peptide synthesizer (Intavis Bioanalytical Instruments AG, Cologne, Germany).

Table 1. Peptide Sequences Constructed for Experimental Analysis

Wild-type	H_2N-KFFEAAAKKFFE-COOH
Capped peptide	CH_3CO-KFFEAAAKKFFE-$CONH_2$
F/A variants	
F2A	K**A**FEAAAKKFFE
F2AF3A	K**AA**EAAAKKFFE
F3AF11A	KF**A**EAAAKKF**A**E
F10F11A	KFFEAAAKK**AA**E
F11A	KFFEAAAKKF**A**
K/R variants	
K8R	KFFEAAA**R**KFFE
K8RK9R	KFFEAAA**RR**FFE
K9R	KFFEAAAK**R**FFE
K1R	**R**FFEAAAKKFFE
K1RK8R	**R**FFEAAA**R**KFFE
K1RK9R	**R**FFEAAAK**R**FFE
K/A variants	
K8A	KFFEAAA**A**KFFE
K8AK9A	KFFEAAA**AA**FFE
K9A	KFFEAAAK**A**FFE
K1A	**A**FFEAAAKKFFE
K1AK8A	**A**FFEAAA**A**KFFE
K1AK9A	**A**FFEAAAK**A**FFE

Cleavage from the resin and deprotection of the peptide were achieved with a mixture containing 9.5 mL of trifluoroacetic acid, 0.25 mL of triisopropylsilane, and 0.25 mL of water at 20 °C for 2 h. After filtration to remove resin, the peptide was precipitated from solution with cold ether. After standing on ice for 10 min, the peptide was pelleted by centrifugation and the ether decanted away. This was repeated once before the peptide was solubilized in 5 mL of water and lyophilized. The crude peptides were analyzed by reverse-phase HPLC−mass spectrometry on an Agilent 1100 Series LC/MSD using a Zorbax Eclipse XDB-C8 rapid resolution HT 3.0 × 50 mm 1.8 μm column, using a 0.8% TFA/water−acetonitrile gradient. Peptides were purified by reverse-phase HPLC on a Perkin-Elmer Series 200 system using a Zorbax 300SB-C8, 21.2 × 250 mm, 7 μm column using a 0.8% TFA/water−acetonitrile gradient.

Peptide solutions were made up to a concentration of 5 mg/mL in either Milli-Q 0.2 μm filtered water or phosphate-buffered saline (PBS) diluted 10× (stock PBS; 19 mM sodium dihydrogen phosphate (NaH_2PO_4), 81 mM disodium hydrogen phosphate (Na_2HPO_4), 1.5 M NaF, pH 7.4). Due to the interference of Cl ions in circular dichroism measurements, PBS was made using NaF instead of NaCl. Samples set up at pH 2 and 12 were dissolved in filtered 10 mM phosphoric acid and 10 mM disodium hydrogen phosphate (Na_2HPO_4), respectively. After addition of solvent, samples were vortexed briefly and centrifuged for 5 min at 13000 rpm to remove any preformed

aggregates using an Eppendorf MiniSpin microcentrifuge (Eppendorf AG, Hamburg, Germany). Any pellet that formed was discarded. Concentration was determined by careful weighing out of the peptide using a microbalance (Sartorius, MA, USA) and calculating the appropriate volume of solvent to be added to achieve the required concentration. Samples were agitated at a speed of 100 rpm at 20 °C for 7 days and examined using the methods indicated below.

Negative Stain Transmission Electron Microscopy (TEM). Four microliters of peptide solution was placed onto a 400 mesh, carbon/Formvar-coated copper grid (Agar Scientific, Essex, U.K.) and incubated at room temperature for 2 min. The grid was washed once using Milli-Q 2 μm filtered water and negatively stained twice with 4 μL of filtered 2% (w/v) uranyl acetate solution. At each stage excess liquid was blotted with filter paper. The grid was allowed to air-dry before examining in a Hitachi 7100 microscope (Hitachi, Germany) operating at 100 kV fitted with a Gatan Ultrascan 1000 CCD camera (Gatan, Abingdon, U.K.). All measurements of TEM images were made using ImageJ.[20]

Intrinsic Phenylalanine Fluorescence. Peptide solutions at a concentration of 5 mg/mL in either PBS or water were diluted to 0.5 mg/mL with the appropriate buffer. Samples were placed in a microvolume cuvette with a 1 cm path length, and fluorescence emission from phenylalanine was measured after 7 days using a Varian Cary Eclipse fluorometer (Varian, Oxford, U.K.) using an excitation wavelength of 265 nm. Water or PBS baselines were subtracted from the data. Triplicate measurements were taken and averaged. Excitation and emission slits were both set to 5 nm. The scan rate was 600 nm/min with 1 nm data intervals and an averaging time of 0.1 s. The voltage on the photomultiplier tube was set to high (800 V). The temperature was maintained at 20 °C using a Peltier device.

Circular Dichroism. Peptide solutions were diluted to 0.5 mg/mL, as for phenylalanine fluorescence experiments, and placed in a 0.02 cm quartz cuvette (Starna, Essex, U.K.). Measurements were taken using a JASCO J-715 spectropolarimeter. The time constant (response) was set to 4 s and the scan rate to 50 nm/min. The bandwidth was 1 nm and the sensitivity set to standard. Scans were performed from 320 to 180 nm with a 0.1 nm data pitch and continuous scan mode. A Peltier device was used to maintain a temperature of 20 °C. Scans were taken in triplicate and the data averaged. Buffer or water baselines were subtracted. Only data recorded with an HT voltage of less than 600 were plotted. All measurements were originally measured in millidegrees and converted to units of mean residue ellipticity (MRE).

X-ray Fiber Diffraction (FD). Peptide samples were prepared for fiber diffraction by placing 20 μL of solution between two wax-filled capillaries and allowed to air-dry at room temperature. The samples were placed on a goniometer head and data collected using a Rigaku rotating anode (Cu Kα) and Raxis IV++ detector (Rigaku, Sevenoaks, U.K.) with specimen to film distances of either 160 or 250 mm. Alternatively, diffraction data were collected on the I24 Microfocus MX beamline at Diamond Light Source, Oxford, U.K., using a wavelength of 0.9778 Å and a distance of 400 mm. Experiments were carried out on at least two separately prepared samples to confirm results.

Data Processing and Unit Cell Optimization. The program CLEARER was used for processing experimental diffraction data and unit cell determination.[21] Diffraction patterns were uploaded into the program and centered. Diffraction settings depended upon the data collection method. For in-house data the sample to detector distance was 160 mm, the wavelength was 1.5419 Å, and the pixel size was 400 μm. For synchrotron data the settings were 312 mm, 0.9778 Å, and 440 μm. Diffraction signal positions were measured by CLEARER, and these were compared to those measured by hand using a function of the program. Using these signal positions, possible unit cells were generated. Initially guessed lattice vectors were defined as a = 4.69 Å, b = 15 Å, and c = 25 Å based on expected unit cell dimensions and $\alpha = \beta = \gamma = 90°$. a was defined as the fiber axis, and b (sheet-spacing) and c (chain length) were optimized. The most intense d-spacings (reflections) measured were entered, and a unit cell was refined.

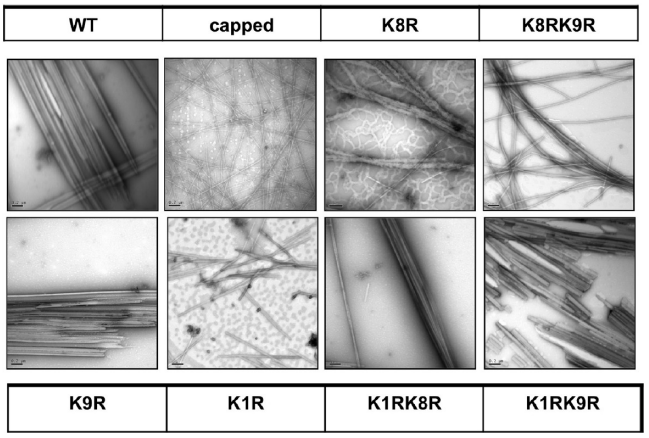

Figure 1. Electron micrographs of the assembled wild-type, capped, and K/R variant peptides in PBS (5 mg/mL). These peptides did not assemble in water at 5 mg/mL. Scale bars are 200 nm.

Modeling of Peptide Structures. Peptide structures were based on the original WT model structure deposited in the Protein Data Bank (3BFI).[13] This structure must be translated by (0.45, −02.14, 1.47), as defined in the header to set the origin and generate symmetry-related objects within the unit cell. The structure was viewed in Pymol, and residues were mutated to arginine or alanine as appropriate for the variants. The structures were then centered within a new unit cell to be tested and symmetry-related objects generated to fill the unit cell.

Calculation of Diffraction Patterns from Model Structures. The model structures were uploaded to diffraction simulation module within CLEARER,[21] and unit cell dimensions determined from unit cell determination analysis were input for diffraction calculation for each of the individual model structures. Diffraction settings were set to match experimental settings, and the diffraction pattern was calculated from the structural models within a defined unit cell. Crystallite size was set to 80 nm and a sampling interval of 1 pixel to give sharp images for the arginine variants (default is 20 nm). Default values were used for all other values. The calculated patterns were displayed and compared to experimental data by comparison of a quadrant of the calculated pattern.

RESULTS

Initially, the assembly characteristics of wild-type and variant peptides were investigated using electron microscopy, and the resulting morphology was evaluated. Each of the peptides shown in Table 1 were incubated for 7 days in buffer or water.

Electron microscopy confirmed that the wild-type peptide forms striated fibrous crystals in PBS but is unable to assemble in water[13] (Figure 1). The pH of the solubilized peptide in water is

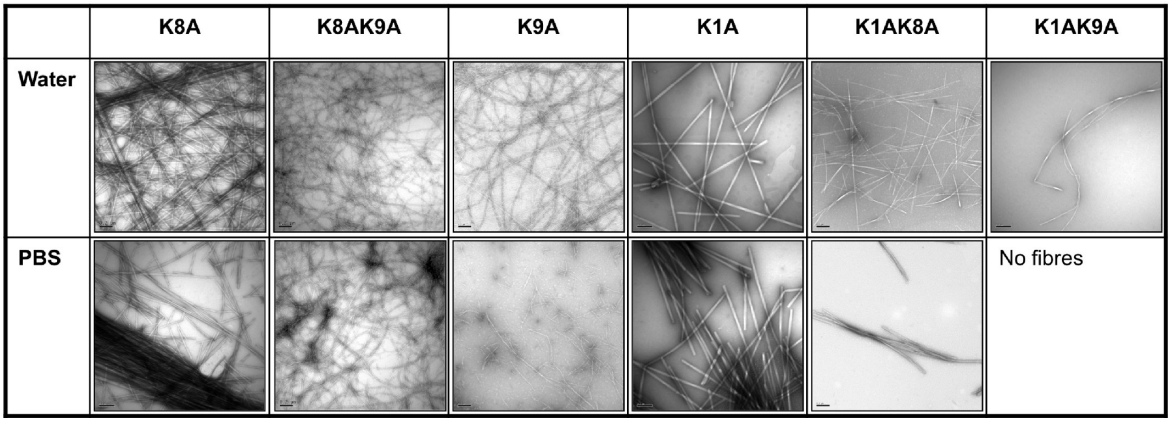

Figure 2. Electron micrographs of assembled K/A variant peptides in water and PBS (5 mg/mL). Scale bars are 200 nm.

3.0 ± 0.5, which results in a charge on the wild-type peptide of +4, whereas in PBS (pH 7.4), the charge is +1. Lopez de la Paz previously reported that a net charge of ±1 allowed for ordered aggregation into amyloid, likely due to reduced repulsion between peptide molecules.[22] These results are consistent with this observation and suggest that for this system charge is an important factor in amyloid assembly, in agreement with previous studies.[22,23] To investigate the effect of pH further, the WT peptide was prepared at a pH of 2 or 12. WT peptide did not assemble with increased net charges (+4 at pH 2 and −3 at pH 12). Charge contributions come from both side chains and the N- and C-termini on the peptides; at high or low pHs the N- and C-termini are not zwitterionic, and therefore peptides will be unable to interact end to end. This may contribute to the inability to assemble. Therefore, to investigate the role of the charged ends, the assembly of a peptide with capped, uncharged ends was examined under the same assembly conditions. Electron microscopy revealed that the capped peptide is able to assemble in PBS but not in water at a concentration of 5 mg/mL, similar to WT. However, increasing the concentration to 10 mg/mL allowed assembly in water (data not shown) while WT does not assemble at 20 mg/mL. This may be due to the reduced charge on the capped peptide in water of +3. When the capped peptide was incubated at pH 2 and 12 at 5 mg/mL (with respective net charges of +3 and −2), small amounts of fibrillar aggregates were observed by electron microscopy (data not shown). However, this appeared to be less efficient and less ordered in morphology than assembly in water. Interestingly, the fibers formed by the capped peptide in PBS at 5 mg/mL differed from those formed by wild-type peptide and did not show lateral striations or lateral aggregation to form larger fibrous crystals (Figure 1). Instead, the capped peptide formed amyloid fibrils with a diameter of around 10 nm, indicating that the charged ends play a role in lateral association of protofilaments in wild type.

To investigate the role of phenylalanine in fibril assembly, peptides with single or double substitutions of phenylalanine for alanine (see Table 1) were incubated in water and PBS. Strikingly, none of the F/A variants were able to assemble under the conditions examined, and circular dichroism confirmed that the solutions contained a random coil conformation (Supporting Information Figure S2). This appears to indicate that all four of the phenylalanine residues are required for assembly and that replacement with alanine renders them assembly incompetent.

In contrast, replacement of the lysine residues with alanine resulted in peptides that were able to assemble in both water and PBS, while the peptides in which lysine was more conservatively replaced with arginine were unable to assemble in water but did form fibrils in PBS, as with the wild-type peptide. Examination of the electron micrograph images (Figures 1 and 2) of the resulting fibrils revealed a variety of morphologies, whereby the K/R variants mostly formed fibrous crystals similar to those formed by wild type in PBS. K/A variants tended to form more amyloid fibrillar-like morphologies in both water and PBS. The ability of the K/A variants to assemble in water is supported by the idea that overall charge is important and lowering net charge to +3 for single mutants and +2 for double mutants in water promotes assembly. The WT peptide model shows lysine−glutamate electrostatic interactions stabilizing the fiber axis direction.[13] However, the resulting morphology of K/A variants indicates that lysine residues may also be involved in lateral association of protofilaments, since these peptides are unable to form crystalline species. In contrast, the K/R peptides retain the same charge properties as wild type. The larger size of the arginine side chain might be expected to disrupt the association between β-sheets, and this was further investigated using biophysical and diffraction methods. Circular dichroism of the peptide assemblies was performed. However, many of the peptide assemblies failed to give consistent results due to differences in solubility and contributions from linear dichroism signals arising from partial alignment.[15]

The previously interpreted molecular structure of wild-type assemblies in PBS indicated interactions between phenylalanine residues both between sheets and along the fiber axis (Supporting Information Figure S1). To investigate this further and to compare to variant assemblies, intrinsic phenylalanine fluorescence was investigated. Monitoring intrinsic fluorescence from other aromatic residues (tryptophan and tyrosine) has been used previously for amyloid systems to explore the conformational environment of certain regions using the fluorescent residue as a probe.[15,24−29] Experiments investigating the intrinsic phenylalanine fluorescence from a short peptide from Aβ, KLVFF, showed a red shift of the emission peak from the normally observed phenylalanine fluorescence maximum.[30] When an excitation wavelength of approximately 260 nm is used, phenylalanine in solution exhibits a fluorescence peak around 280 nm.[31] However, the investigators found that fibrils formed from KLVFF gave fluorescence emission spectra that were shifted from this position to a longer wavelength of 313 nm, which they attributed to $\pi-\pi$ stacking between aromatic residues.[30] As this interaction is also proposed to feature in the model of the WT structure, the intrinsic fluorescence from

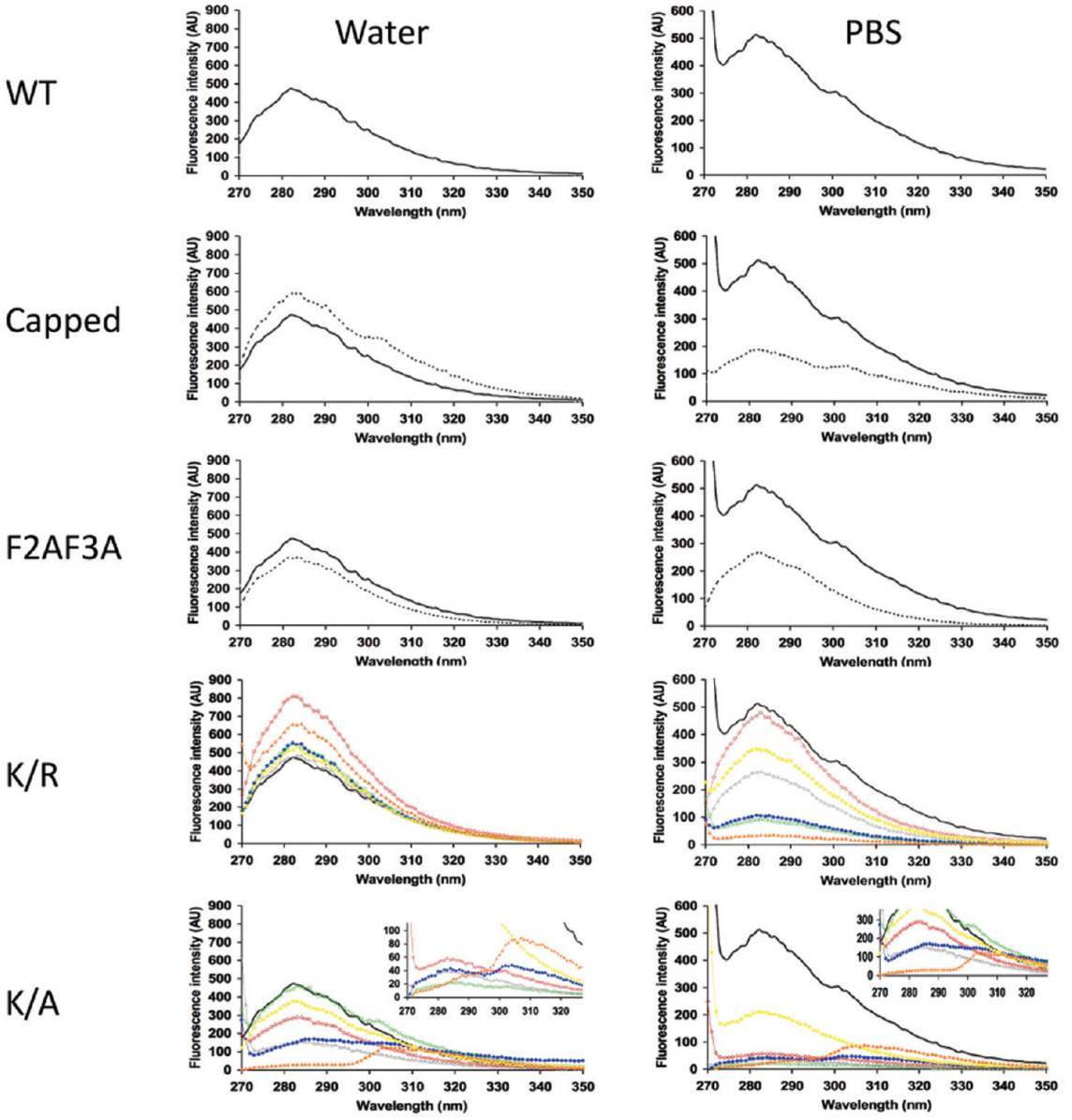

Figure 3. Phenylalanine fluorescence of wild-type and variant peptides following incubation in water and PBS at 5 mg/mL. WT is shown as a solid black line in all figures. K8A, red open circles; K8AK9A, blue closed circles; K9A, green open squares; K1A, yellow closed squares; K1AK8A, gray open triangles; K1AK9A, orange closed triangles.

phenylalanine was measured to corroborate the $\pi-\pi$ stacking and thus the integrity of the published model[13] and once again determine whether the variants differed in this respect to the WT.

Phenylalanine fluorescence from the WT peptide (Figure 3) resulted in a peak at 303 nm from the PBS sample that is not observed in the water sample. This may arise from the stacking of the phenylalanine residues within the fibrous crystals, which is supported by the model structure. The position of this peak differs slightly from those reported previously,[30] but as it is only present in the sample that assembled, we propose that it is attributable to $\pi-\pi$ stacking. Investigation of assemblies of capped peptide in water and in PBS showed an intrinsic phenylalanine fluorescence peak at 282 nm with a shoulder centered around 303 nm, suggesting assembly in water that leads to association of phenylalanine residues (although no assemblies were visible at the concentration of 5 mg/mL in water but were observed at higher concentrations). Consistent with electron microscopy results showing that F/A variants do not assemble in water, CD spectra showed a random coil signal at 195 nm (Supporting Information Figure S2), and intrinsic phenylalanine fluorescence showed no additional peak.

None of the K/R variants in either water or PBS showed the shoulder at 303 nm by intrinsic phenylalanine fluorescence. This seems to suggest that although the conformation of the peptide and its ability to assembly in PBS and not water are similar to wild type, the close association of the phenylalanine residues that gives rise to the 303 nm peak is disrupted, possibly by accommodation of the larger side chain. TEM revealed that K/A variants were able to fibrillize in water and that in PBS they did not form WT-like crystals, but narrow fibrils. Intrinsic phenylalanine fluorescence revealed the 303 nm peak only for K8A (PBS), K9A (PBS and water), and K1A (water) and a relatively

dx.doi.org/10.1021/bi101936c |*Biochemistry* 2011, 50, 2061–2071

Table 2. Summary of Results[a]

	TEM		phenylalanine fluorescence (303 nm)		fiber diffraction		model	
	water	PBS	water	PBS	water	PBS	water	PBS
WT	−	++	−	+	−	Makin[c]	−	Makin[c]
capped	−	+++	+	+	+[b]	−	−	−
F/A	−	−	−	−	−	−	−	−
K8R	−	+	−	−	−	−	−	−
K8RK9R	−	++	−	−	−	+	−	−
K9R	−	++	−	−	−	+	−	−
K1R	−	++	−	−	−	−	−	−
K1RK8R	−	++	−	−	−	+	−	+
K1RK9R	−	+++	−	−	−	+	−	−
K8A	+++	+++	−	+	+	+	−	+
K8AK9A	+++	+++	+	+	+	−	−	−
K9A	+++	++	+	+	+	−	−	−
K1A	+++	++	+	−	+	−	−	−
K1AK8A	++	+	−	−	−	−	−	−
K1AK9A	+	−	+	+	−	−	−	−

[a] For TEM images, where no material is observed, a dash is shown. Where fibrils were observed, their relative estimated quantity is given by + (very few fibrils) to +++ (high fibril concentrations). Representative TEM images are shown in Figures 1 and 2. Those samples that showed a phenylalanine fluorescence peak at 303 nm are indicated with +. Similarly, samples that diffracted and were modeled are indicated by + and are shown in Figures 4 and 6. [b] Capped peptide prepared at 10 mg/mL. [c] See ref 13.

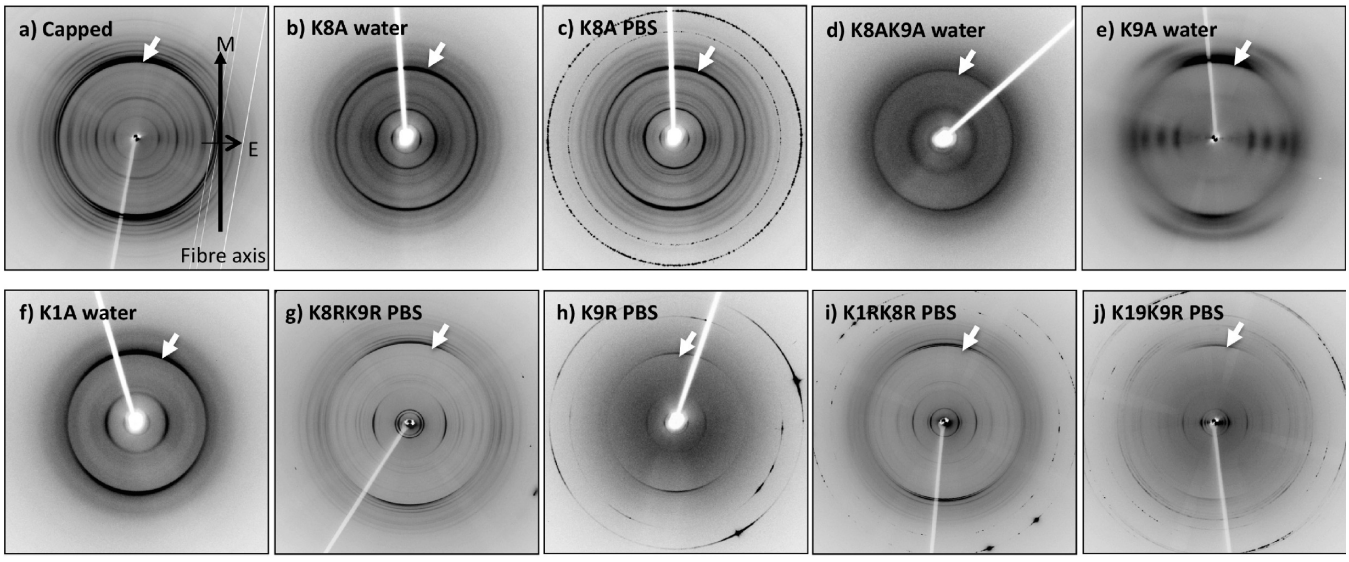

Figure 4. X-ray fiber diffraction patterns of K/A and K/R variants that aligned. Fiber axes are vertical. The position of the strong 4.7 Å meridional reflection is highlighted by white arrows. The spotted rings arise from PB crystals forming from the buffer.

strong peak for K8AK9A in water and K1AK9A in both solvents, indicating that in these fibrils the association of phenylalanine residues is maintained. The latter result was somewhat unexpected given that very few fibers were observed by TEM in water and none at all in PBS but, in a similar manner to the capped peptide, may point toward peptide association and $\pi-\pi$ stacking from small, oligomeric species. The lack of any peak at 303 nm for K8A in water, K1A in PBS, and K1AK8A in both solvents suggests that $\pi-\pi$ stacking might be disrupted in these assemblies. The results of TEM, phenylalanine fluorescence, and also fiber diffraction analysis are summarized in Table 2.

X-ray fiber diffraction reveals information regarding the repeating units within the amyloid-like fibrils and can be analyzed to arrive at unit cell dimensions to enable model structures to be constructed.[32] We attempted to align all of the fibril-forming variants to form fiber samples for examination by X-ray diffraction. All of the diffraction patterns obtained from fibril-forming samples gave characteristic cross-β patterns; however, some gave additional information and are shown in Figure 4. First glance reveals that the diffraction patterns obtained from K/R variants show a series of very sharp reflections, and this is highly consistent with the observation of fibrous crystals by electron microscopy similar to that obtained from the WT peptide. In contrast, patterns from capped and K/A peptides showed more diffuse reflections, and this is consistent with the appearance of fibrils by TEM. The positions of the reflections were measured

Table 3. Unit Cell Determination

	WT PBS	capped water	K8A PBS	K9A water	K8RK9R PBS	K1RK8R PBS	K1RK9R PBS
b	**21.3**	21.80	21.60	18.35	21.26	22.80	21.93
c	**48.1**	31.05	47.92	38.92	51.71	50.12	53.30

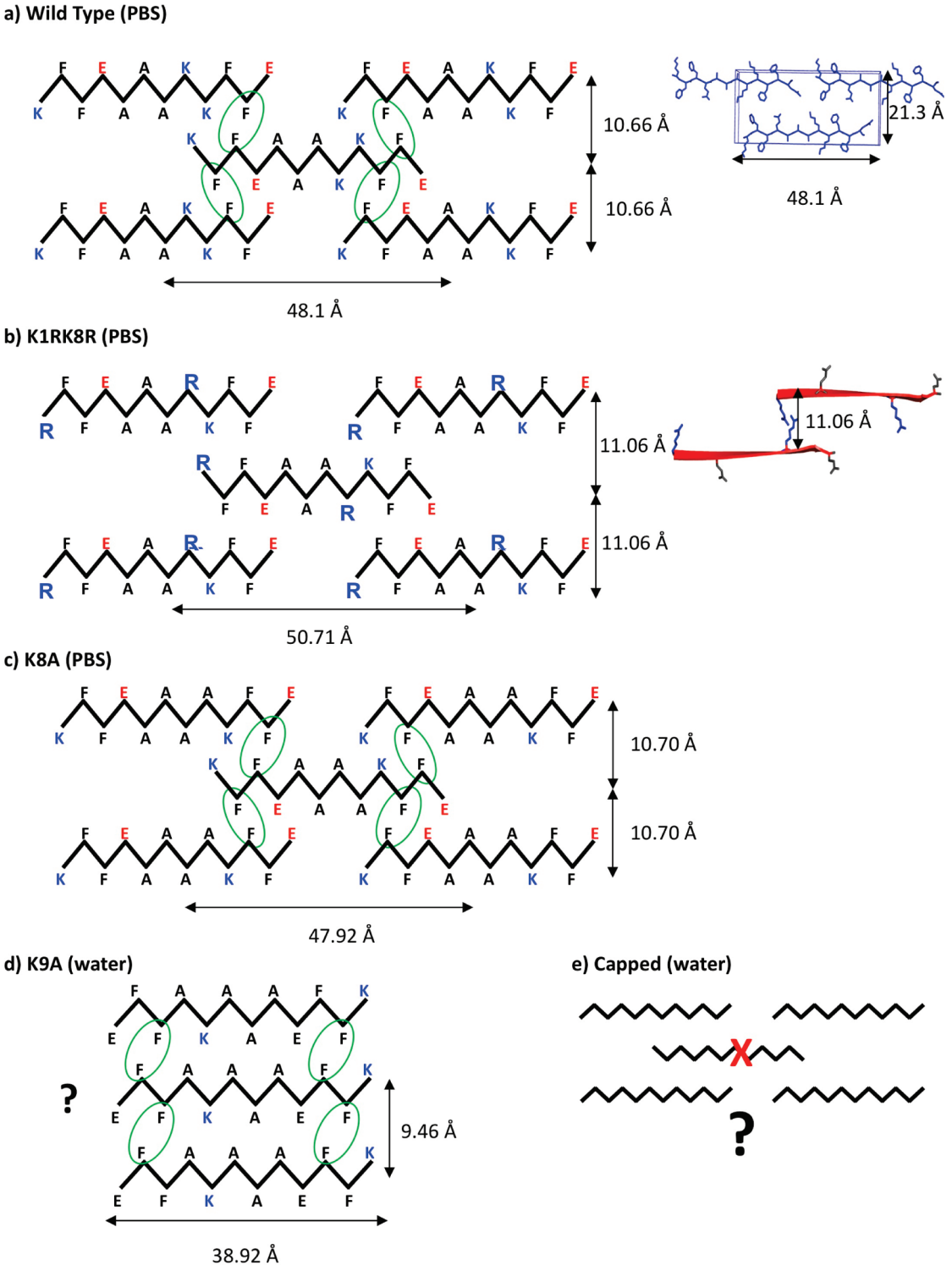

Figure 5. Schematic showing model structures arising from structural analysis of fiber diffraction patterns and unit cell determination.

and are shown in Supporting Information Table S1. The reflections were then analyzed using CLEARER[21] to explore possible unit cell dimensions (details shown in Supporting Information Table S2). This analysis allows us to determine how similar or

dx.doi.org/10.1021/bi101936c |*Biochemistry* 2011, 50, 2061–2071

different the structures of the variants are when compared to the WT structure. Only those patterns with sufficient information could be indexed, and further analysis of patterns from fibrils of K8AK9A, K1A, and K9R were not attempted. The determined unit cell dimensions for those patterns that showed a number of signals on the equator are shown in Table 3. Further information on how the unit cells were determined can be found in the Supporting Information (Tables S1 and S2).

The capped variant showed some similarities to WT patterns, specifically in the chain length direction, but could not be indexed to the same unit cell as WT. This may indicate that the arrangement of the peptides differs from the WT arrangement and that this difference arises from the removal of charged ends. These clearly play a role in lateral association that gives rise to the crystalline packing afforded by the WT peptide. The K8A pattern could be indexed to a cell 9.5 Å × 21.6 Å × 47.9 Å, which is very similar to the WT unit cell as shown in Table 3 and indicates that despite the effects of the alanine substitution that results in fibrillar, rather than crystalline structures, the structure is maintained in this variant. K8A in PBS produced a diffraction pattern with more detail and was used for unit cell analysis. The substitution K9A appears to be more disruptive, and the unit cell determination gave smaller dimensions (9.5 Å × 18.3 Å × 38.9 Å), suggesting that the structural packing is more condensed, arising from the removal of K9. A schematic of possible changes to the structures compared to wild type is shown in Figure 5.

The replacement of lysine with arginine in the double mutants mostly resulted in ordered, crystalline-like fibrils that gave highly ordered diffraction patterns. It is interesting to note that only double mutations gave rise to ordered patterns. Unit cell determinations from K8RK9R, K1RK8R, and K1RK9R were similar (around 9.5 Å × 21−22 Å × 51−53 Å), suggesting that these peptides are all accommodated within similar packing arrangements. Consideration of how this impacts on the structure of the peptides is shown in the schematic in Figure 5 for K1RK8R and suggests that the intersheet spacing increases from 10.66 Å (for WT) to around 11 Å for the K/R mutants. This allows the larger side chain to be accommodated within the structure without significant changes to the packing. However, this slightly larger sheet spacing could explain the lack of any red-shifted phenylalanine fluorescence signal for all R variants, since this increase in spacing could disrupt the association that might give rise to this signal. Similarly, the majority of K/A variants showed smaller β-sheet spacings because the less bulky alanine allows the sheets to come closer together. K8A gives a similar β-sheet spacing to WT, while it seems that K9 is influential in determining this distance as the greatest reduction was in K8AK9A and K9A samples.

The model for the WT peptide has a brick-like arrangement of peptides,[13] and fiber diffraction supports a similar arrangement for the K/R variants except with increased chain length and sheet spacing dimensions (Figure 5a,b). It would also seem that K8A has a similar underlying structure (Figure 5c). From these data, K9A and the capped peptide do not appear to adopt this arrangement. The very narrow width of the filaments formed by K9A constrains the models that could be proposed. The length of one 12 residue peptide chain is approximately 42 Å, and the width of the fibers formed by K9A is approximately 50 Å. Therefore, it would seem more likely that in these fibers the peptides are arranged in a similar fashion to that shown in Figure 5d. Due to the shorter *c* distance in the capped unit cell, no peptide arrangement has been proposed for the capped peptide. It appears that the change in C- and N-terminal charges has a significant effect on the arrangement of the peptides in the fibrils.

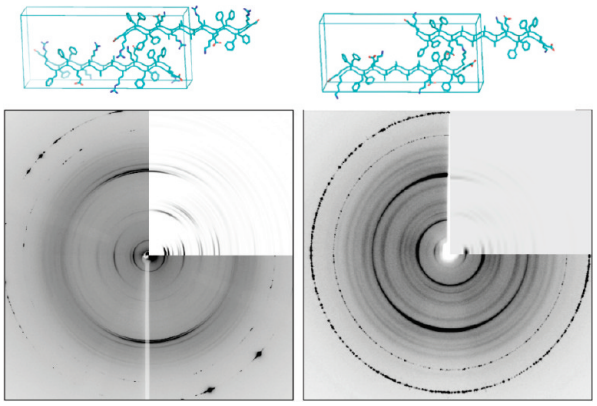

Figure 6. Model structures for two variants, K1RK8R (right) and K8A (left), showing comparison between experimental and calculated diffraction patterns in the quadrant insert. The model structures within unit cells are shown above each fiber pattern. The calculated patterns show excellent agreement with the experimental data.

In order to test the suggested minor changes to the structures, K8A and K1RK8R models were generated within the suggested unit cells (Table 3) and corresponding diffraction patterns were calculated using CLEARER[21] and compared to the experimental data. The close similarities between the experimental and calculated patterns are shown in Figure 6, indicating that altering the cell dimensions, but not the arrangement, significantly produces models that are consistent with the experimentally observed data.

DISCUSSION

The aim of this work was to determine how certain amino acids influence assembly and resulting fiber structure using the peptide KFFEAAAKKFFE as a basis for comparison for a selection of variants constructed. The difficulty in using X-ray crystallography as a method for structure determination of amyloid-forming peptides is well-known, and hence in many cases other biophysical methods are used to gain structural clues.[33] Here, a collection of techniques were used to assess the extent to which the variants differed structurally from the WT peptide and how the peptides might be arranged in any assemblies that formed.

The morphologies of the fibrils and fibrous crystals did appear to vary between the different variants, indicating a modulation of protofilament packing arising from the amino acid substitutions in terms of charge and amino acid side chain size. Additionally, it appears that particular substitutions may have more of an effect than others, namely, that phenylalanine seems to be important in allowing fibrillization to proceed.[18]

Net charge and solution pH seem to be important determinants, in line with previous observations.[23,34,35] The WT peptide cannot assemble in water (where the net charge is +4) at any concentration tested up to 20 mg/mL. This is likely to be because of the high overall net charge leading to repulsion and because of the unbalanced charges on the N- and C-termini, which will be protonated and uncharged, respectively. Capping the ends removes this latter effect and still no assembly is seen at 5 mg/mL despite the lower net charge of +3. However, raising the concentration of the capped peptide to 10 or 20 mg/mL results in an assembly-competent peptide that forms fibrils in water. The

charges on the N- and C-termini, therefore, seem to contribute to lateral association, and removal results in an alternative structure (narrow fibrils), whereas overall net charge and concentration affect simply whether peptides will assemble or not. Lower net charges result in greater assembly potential. Peptide solubility is also important and may be affected not only by differences in net charge but also by chemical composition and screening effects induced during aggregation.

In these experiments, the presence of all four phenylalanine residues is essential for assembly. However, intrinsic phenylalanine fluorescence data indicate that very close aromatic interactions, although possibly present in many cases, might contribute to but not be essential for stabilization of the structure. These results suggest that hydrophobicity, and not aromaticity, of phenylalanine may be the primary driving force of assembly. Although alanine is hydrophobic, it is less so compared to phenylalanine.[36] Results from short amylin-derived peptides and islet amyloid polypeptide where phenylalanine was substituted for either leucine or alanine showed that the F/L peptides were far more amyloidogenic than the F/A peptides, leading the investigators to conclude that aromaticity is not fundamental in amyloid formation.[37,38] However, the authors do acknowledge that the aromatic character of phenylalanine does have an influence on assembly and the resulting ultrastructure.[38] As we do not see assembly when phenylalanine is replaced with alanine, we can conclude that this is due to either a reduction in hydrophobicity or abolishment of aromaticity. Nevertheless, the intrinsic phenylalanine fluorescence data suggest that aromaticity does play a structural role. A feature of most of the crystal structures produced by the Eisenberg group is the steric zipper where side chains interdigitate in a dry interface due to a high complementarity.[11] This does not appear to be the case for the fibrous crystals formed by KFFEAAAKKFFE. Instead, the crystalline structure appears to be generated because of the combination of features of the peptide, namely, the charged ends, the location of the ionizable K and E residues, and the presence and position of the hydrophobic, aromatic phenylalanine residues.

Replacing lysine with alanine had the second most dramatic effect, after the F/A variants. K/A variants were able to fibrillize in water at 5 mg/mL, possibly due to the combination of a lower net charge and the replacement of lysine with the more hydrophobic alanine. In PBS, fibrils only, and not crystals, formed despite the zwitterionic N- and C-terminal charges. Lysine may also be involved in lateral association as its removal hinders this process and the formation of crystalline species. In addition, a lower net charge (0 or −1) could cause backbone hydrogen bonding in the fiber axis direction to proceed without competition from charge repulsion. In some of the variants in PBS the salt bridge would be affected by replacement of lysine with alanine, particularly in the K1AK9A variant. Indeed, this peptide does not assemble in PBS. However, in water, in all cases no salt bridge would be able to form as the charge on the glutamate residues will be zero. Therefore, it is possible that in water the fibrils that are formed by the K/A variants have a very different structure that does not feature a salt bridge, nor in some cases $\pi-\pi$ stacking, as a stabilizing force. Replacing lysine with arginine had less impact structurally, but nevertheless effects were significant, and the location of the substitution appeared to be important.

Interpretation of the biophysical data gives us clues regarding how these assemblies show similarities or differences from the WT fibrous crystals and each other. Intrinsic phenylalanine fluorescence shows that there are likely to be subtle differences even among similar structures. Therefore, it may be concluded that while some peptides form an overall similar architecture in terms of peptide packing, the variation induced by replacing either K1 or K9 with alanine affects the interaction between phenylalanine residues.

Other residues are also able to affect side chain interactions. Here, the presence of arginine instead of lysine appears to affect the interactions between phenylalanine residues. The similar macroscopic morphology and unit cell dimensions suggest that in general these variants are similar to the WT peptide but that $\pi-\pi$ stacking might not be fundamental for maintenance of the structure.

The lack of a fluorescence peak at 303 nm is evident in other samples. K8A appears similar in water and PBS from TEM and FD results. However, intrinsic phenylalanine fluorescence data suggest that these residues are more closely positioned to each other in the fibrils that form in PBS, as no 303 nm signal is observed for K8A in water. FD would not pick up on such subtle differences in side chain packing; rather it serves to provide information on how the peptides are packed overall on a longer scale range.

These results show how changes in chemical composition in short peptides such as these can have dramatic effects on assembly and structure. Understanding precisely how sequence influences structure using model systems may help to understand structure−function relationships. Recent work by Campioni et al. has highlighted how toxicity may be dependent on structure and that surface hydrophobic exposure in oligomeric species may be responsible for toxic effects.[39] This work reveals the essential role of phenylalanine in amyloid assembly but also that peptides are able to form alternative structures and adds to the knowledge regarding polymorphism in amyloid. The wide range of morphologies shown here and their vastly different underlying structural characteristics illustrate how peptides capable of forming amyloid structures are adaptable and respond to the constraints imposed upon them to form alternative structures. The results also highlight how altering the chemical composition of peptides can in some cases alter assembly and structure more than is anticipated, as illustrated by the K/R variants. Insights from experiments on short peptides such as those shown here contribute to our understanding of the specific activities of different amyloid structures and allow exploitation from an industrial and design perspective.

■ ASSOCIATED CONTENT

Supporting Information. Additional experimental procedure, tables of diffraction signals and cell determination, and figures showing the original structure of KFFEAAAKKFFE and CD spectra for F/A mutants. This material is available free of charge via the Internet at http://pubs.acs.org.

■ AUTHOR INFORMATION

Corresponding Author

*E-mail: L.C.Serpell@sussex.ac.uk. Tel/Fax: +44 1273 877363.

Present Addresses

[§]Laboratory of Persistent Viral Diseases, Rocky Mountain Laboratories, NIAID, NIH, 903 S. 4th St., Room 2102, Hamilton, MT 59840.

Funding Sources
This work is supported by funding from the BBSRC and Alzheimer's Research Trust.

■ ACKNOWLEDGMENT

The authors thank Professor Alison Rodger and Dr. Matthew Hicks for helpful advice and discussion and Dr. Julian Thorpe for help with transmission electron microscopy. The authors gratefully acknowledge the beam scientists at I24 Diamond light source for valuable help in data collection. We gratefully acknowledge the help of Dr. Thomas Williams for valuable discussions and critical reading of the manuscript.

■ ABBREVIATIONS

TEM, transmission electron microscopy; WT, wild type; PBS, phosphate-buffered saline; CD, circular dichroism; MRE, mean residue ellipticity; HT, high tension; FD, fiber diffraction.

■ REFERENCES

(1) Selkoe, D. J. (2000) Toward a comprehensive theory for Alzheimer's disease. Hypothesis: Alzheimer's disease is caused by the cerebral accumulation and cytotoxicity of amyloid beta-protein. *Ann. N. Y. Acad. Sci. 924*, 17–25.

(2) Fowler, D. M., Koulov, A. V., Balch, W. E., and Kelly, J. W. (2007) Functional amyloid—from bacteria to humans. *Trends Biochem. Sci. 32*, 217–224.

(3) Maji, S. K., Ogorzalek Loo, R. R., Inayathullah, M., Spring, S. M., Vollers, S. S., Condron, M. M., Bitan, G., Loo, J. A., and Teplow, D. B. (2009) Amino acid position-specific contributions to amyloid beta-protein oligomerization. *J. Biol. Chem. 284*, 23580–23591.

(4) Dobson, C. M. (2003) Protein folding and misfolding. *Nature 426*, 884–890.

(5) Rousseau, F., Schymkowitz, J., and Serrano, L. (2006) Protein aggregation and amyloidosis: confusion of the kinds?. *Curr. Opin. Struct. Biol. 16*, 118–126.

(6) Jimenez, J. L., Tennent, G., Pepys, M., and Saibil, H. R. (2001) Structural diversity of ex vivo amyloid fibrils studied by cryo-electron microscopy. *J. Mol. Biol. 311*, 241–247.

(7) Wilson, L. M., Mok, Y. F., Binger, K. J., Griffin, M. D., Mertens, H. D., Lin, F., Wade, J. D., Gooley, P. R., and Howlett, G. J. (2007) A structural core within apolipoprotein C-II amyloid fibrils identified using hydrogen exchange and proteolysis. *J. Mol. Biol. 366*, 1639–1651.

(8) Hoshino, M., Katou, H., Hagihara, Y., Hasegawa, K., Naiki, H., and Goto, Y. (2002) Mapping the core of the beta(2)-microglobulin amyloid fibril by H/D exchange. *Nat. Struct. Biol. 9*, 332–336.

(9) Williams, A. D., Portelius, E., Kheterpal, I., Guo, J. T., Cook, K. D., Xu, Y., and Wetzel, R. (2004) Mapping abeta amyloid fibril secondary structure using scanning proline mutagenesis. *J. Mol. Biol. 335*, 833–842.

(10) Zhang, A., Qi, W., Good, T. A., and Fernandez, E. J. (2009) Structural differences between Abeta(1−40) intermediate oligomers and fibrils elucidated by proteolytic fragmentation and hydrogen/deuterium exchange. *Biophys. J. 96*, 1091–1104.

(11) Sawaya, M. R., Sambashivan, S., Nelson, R., Ivanova, M. I., Sievers, S. A., Apostol, M. I., Thompson, M. J., Balbirnie, M., Wiltzius, J. J., McFarlane, H. T., Madsen, A. O., Riekel, C., and Eisenberg, D. (2007) Atomic structures of amyloid cross-beta spines reveal varied steric zippers. *Nature 447*, 453–457.

(12) Nelson, R., and Eisenberg, D. (2006) Recent atomic models of amyloid fibril structure. *Curr. Opin. Struct. Biol. 16*, 260–265.

(13) Makin, O. S., Atkins, E., Sikorski, P., Johansson, J., and Serpell, L. C. (2005) Molecular basis for amyloid fibril formation and stability. *Proc. Natl. Acad. Sci. U.S.A. 102*, 315–320.

(14) Madine, J., Copland, A., Serpell, L. C., and Middleton, D. A. (2009) Cross-beta spine architecture of fibrils formed by the amyloidogenic segment NFGSVQFV of medin from solid-state NMR and X-ray fiber diffraction measurements. *Biochemistry 48*, 3089–3099.

(15) Marshall, K. E., Hicks, M. R., Williams, T. L., Hoffmann, S. V., Rodger, A., Dafforn, T. R., and Serpell, L. C. (2010) Characterizing the assembly of the Sup35 yeast prion fragment, GNNQQNY: structural changes accompany a fiber-to-crystal switch. *Biophys. J. 98*, 330–338.

(16) Tjernberg, L., Hosia, W., Bark, N., Thyberg, J., and Johansson, J. (2002) Charge attraction and beta propensity are necessary for amyloid fibril formation of tetrapeptides. *J. Biol. Chem. 277*, 43243–43246.

(17) Hosia, W., Bark, N., Liepinish, E., Tjernberg, A., Persson, B., Hallen, D., Thyberg, J., Johansson, J., and Tjernberg, L. (2004) Folding into a beta-hairpin can prevent amyloid fibril formation. *Biochemistry 43*, 4655–4661.

(18) Gazit, E. (2002) A possible role for pi-stacking in the self-assembly of amyloid fibrils. *FASEB J. 16*, 77–83.

(19) Kim, W., and Hecht, M. H. (2006) Generic hydrophobic residues are sufficient to promote aggregation of the Alzheimer's Abeta42 peptide. *Proc. Natl. Acad. Sci. U.S.A. 103*, 15824–15829.

(20) Abramoff, M. D., Magelhaes, P. J., and Ram, S. J. (2004) Image Processing with ImageJ. *Biophotonics Int. 11*, 36–42.

(21) Makin, O. S., Sikorski, P., and Serpell, L. C. (2007) CLEARER: a new tool for the analysis of X-ray fibre diffraction patterns and diffraction simulation from atomic structural models. *Appl. Crystallogr. 40*, 966–972.

(22) Lopez De La Paz, M., Goldie, K., Zurdo, J., Lacroix, E., Dobson, C. M., Hoenger, A., and Serrano, L. (2002) De novo designed peptide-based amyloid fibrils. *Proc. Natl. Acad. Sci. U.S.A. 99*, 16052–16057.

(23) Calamai, M., Taddei, N., Stefani, M., Ramponi, G., and Chiti, F. (2003) Relative influence of hydrophobicity and net charge in the aggregation of two homologous proteins. *Biochemistry 42*, 15078–15083.

(24) Padrick, S. B., and Miranker, A. D. (2001) Islet amyloid polypeptide: identification of long-range contacts and local order on the fibrillogenesis pathway. *J. Mol. Biol. 308*, 783–794.

(25) Sudhakar, K., Wright, W. W., Williams, S. A., Phillips, C. M., and Vanderkooi, J. M. (1993) Phenylalanine fluorescence and phosphorescence used as a probe of conformation for cod parvalbumin. *J. Fluoresc. 3*, 57–64.

(26) Dusa, A., Kaylor, J., Edridge, S., Bodner, N., Hong, D. P., and Fink, A. L. (2006) Characterization of oligomers during alpha-synuclein aggregation using intrinsic tryptophan fluorescence. *Biochemistry 45*, 2752–2760.

(27) Kihara, M., Chatani, E., Iwata, K., Yamamoto, K., Matsuura, T., Nakagawa, A., Naiki, H., and Goto, Y. (2006) Conformation of amyloid fibrils of beta2-microglobulin probed by tryptophan mutagenesis. *J. Biol. Chem. 281*, 31061–31069.

(28) Touchette, J. C., Williams, L. L., Ajit, D., Gallazzi, F., and Nichols, M. R. (2010) Probing the amyloid-beta(1−40) fibril environment with substituted tryptophan residues. *Arch. Biochem. Biophys. 494*, 192–197.

(29) Maji, S. K., Amsden, J. J., Rothschild, K. J., Condron, M. M., and Teplow, D. B. (2005) Conformational dynamics of amyloid beta-protein assembly probed using intrinsic fluorescence. *Biochemistry 44*, 13365–13376.

(30) Krysmann, M. J., Castelletto, V., Kelarakis, A., Hamley, I. W., Hule, R. A., and Pochan, D. J. (2008) Self-assembly and hydrogelation of an amyloid peptide fragment. *Biochemistry 47*, 4597–4605.

(31) Du, H., Fuh, R. A., Li, J., Corkan, A., and Lindsey, J. S. (1998) PhotochemCAD: A computer-aided design and research tool in photochemistry. *Photochem. Photobiol. 68*, 141–142.

(32) Makin, O. S., and Serpell, L. C. (2005) X-ray diffraction studies of amyloid structure, in *Amyloid proteins: methods and protocols* (Sigurdsson, E. M., Ed.) pp 67−80, Humana Press, Totowa, NJ.

(33) Bartlett, A. I., and Radford, S. E. (2009) An expanding arsenal of experimental methods yields an explosion of insights into protein folding mechanisms. *Nat. Struct. Mol. Biol. 16*, 582–588.

(34) Schmittschmitt, J. P., and Scholtz, J. M. (2003) The role of protein stability, solubility, and net charge in amyloid fibril formation. *Protein Sci. 12*, 2374–2378.

(35) Schneider, J. P., Pochan, D. J., Ozbas, B., Rajagopal, K., Pakstis, L., and Kretsinger, J. (2002) Responsive hydrogels from the intramolecular folding and self-assembly of a designed peptide. *J. Am. Chem. Soc. 124*, 15030–15037.

(36) Cornette, J. L., Cease, K. B., Margalit, H., Spouge, J. L., Berzofsky, J. A., and DeLisi, C. (1987) Hydrophobicity scales and computational techniques for detecting amphipathic structures in proteins. *J. Mol. Biol. 195*, 659–685.

(37) Tracz, S. M., Abedini, A., Driscoll, M., and Raleigh, D. P. (2004) Role of aromatic interactions in amyloid formation by peptides derived from human Amylin. *Biochemistry 43*, 15901–15908.

(38) Marek, P., Abedini, A., Song, B., Kanungo, M., Johnson, M. E., Gupta, R., Zaman, W., Wong, S. S., and Raleigh, D. P. (2007) Aromatic interactions are not required for amyloid fibril formation by islet amyloid polypeptide but do influence the rate of fibril formation and fibril morphology. *Biochemistry 46*, 3255–3261.

(39) Campioni, S., Mannini, B., Zampagni, M., Pensalfini, A., Parrini, C., Evangelisti, E., Relini, A., Stefani, M., Dobson, C. M., Cecchi, C., and Chiti, F. (2010) A causative link between the structure of aberrant protein oligomers and their toxicity. *Nat. Chem. Biol. 6*, 140–147.